
	Deliverable ID:	Preparation date:
	D3.5	03 March 2020
 <p>Terahertz based Ultra High Bandwidth Wireless Access Networks</p>	Milestone: Final ¹	
	Title:	
	<p>Characterization report of phase distribution PIC</p>	
	Editor/Lead beneficiary (name/partner):	
	Marco Garcia/VLC Photonics	
	Internally reviewed by (name/partner):	
Johannes Eckhardt/University Braunschweig Luís Pessoa/INESC		
Approved by:		
Luis González/UCL		
Dissemination level		
PU	Public	X
CO	Confidential, only for members of the consortium (including Commission Services)	

Revisions				
Version	Date	Author	Organisation	Details
0.1	14-12-2018	Marco Garcia	VLC Photonics	
0.2	09-01-2019	Alberto Hinojosa	VLC Photonics	Title page
0.3	25-01-2019	Marco Garcia	VLC Photonics	Changes from internal review
1.1	29-12-2019	Alberto Hinojosa	VLC Photonics	Minor changes requested by the reviewers (see section 4)
1.2	03-03-2020	Alberto Hinojosa	VLC Photonics	Clean version

Table of contents

Table of contents	2
1 Executive summary	3
2 Introduction	4
2.1 Summary	4
2.2 Relationships with other deliverables	4
2.3 Contributors	4
3 Characterization.....	4
3.1 Introduction.....	4
3.1.1 Photonic integrated circuit.....	4
3.2 Characterization of test structures.....	5
3.2.1 Single waveguides	5
3.2.2 Multi-mode interferometer 1x2	6
3.2.3 Multi-mode interferometer 2x2	6
3.2.4 MZI 1x2.....	7
3.3 Characterization of system structures	7
4 Future work	10
5 Conclusion.....	11



1 Executive summary

The TERAPOD project aims to provide the technology for future Data Centre ultra-fast wireless links. A crucial part of this approach is the capacity of such systems to find and establish links between devices. In order to optimise the performance and reduce the power consumption, TERAPOD is developing a beam forming system which allows efficient and low-power multi-device links by optically controlling the directionality of the antenna. Such optical control is based on photonic integrated circuits (PICs).

This document provides the results from the measurements of the photonic integrated circuit (PIC) previously designed and reported in Deliverable D3.3.

First, an overview of the fabricated PIC is provided. After that, a description of the test structures and their measured performance is presented. Finally, as the phase distribution system consist of a 4-branched circuit where all branches are considered equal, several basic measurements of the system are presented for a single branch as representation of the complete system. Some comments on the functionality are added within the conclusions.



2 Introduction

2.1 Summary

In the present deliverable the initial results from experimental measurements of the phase distribution Photonic Integrated circuit (PIC) described in deliverable D3.3 are presented. This PIC is intended to demonstrate the capacity to control the delay and amplitude of two laser signals separated by 100GHz coming from a single input to 4 antenna elements constituting an antenna array. The delay is achieved by means of tunable ring resonators while the amplitude is achieved by cascaded 1x2 tunable Mach-Zehnder interferometers in a tree fashion to achieve 1x4 splitting.

The PIC to be characterized consists of 3 sections, two containing test structures, located at north and south of the PIC as shown in Fig. 1. The third section containing the full 4 delay-line system is located in the center of the PIC (named in this document as the “complete system”). The complete system includes two extra waveguides, one north and one south, to assist during the alignment for characterization and for the packaging.

First the measurements from test straight waveguides are presented. Followed by a multimode interferometer (MMI) 1x2 and MMI 2x2. This section finishes with the measurements on the Mach-Zehnder Interferometer (MZI) used to balance the power between outputs.

2.2 Relationships with other deliverables

The measurements presented in this document relates to the following deliverables:

- D3.3 - M6 - Design report of phase distribution PIC.:

The present deliverable is a continuation of the work presented in deliverable D3.3, where a description of the design to be fabricated is given. In the current document, the results from its fabrication and the experimental measurements are shown.

2.3 Contributors

The following partners have contributed to this deliverable:

- VLC – Photonics – Marco Garcia
- University College London (UCL) - Cyril Renaud & Luis Gonzalez
- BAY Photonics – Larry Clark
- INESC – Luis Pessoa

3 Characterization

3.1 Introduction

3.1.1 Photonic integrated circuit

A picture of one out of eight fabricated chips is presented in Fig.1. The north (blue) and south (red) areas correspond to the test structures. These structures are used within the phase distribution system and by including them independently in the die, we can characterize their overall performance directly. This is required to discard possible fabrication errors.

The phase distribution system, as mention in deliverable D3.3, aims to distribute and control the input laser light to four different outputs, which will be couple into an array of four antenna elements. Firstly, the power is divided into four outputs by means of a 2-stage MZI-based power splitter. The



MZIs are thermally controlled which allows the antenna array radiation pattern to be modified. Finally, the pointing direction of the radiation pattern is controlled by the delay of the signal towards each antenna element by means of micro-ring resonators providing true-time delay.

The area surrounded in purple in Fig.7 encompasses the phase-distribution system plus the alignment waveguides.

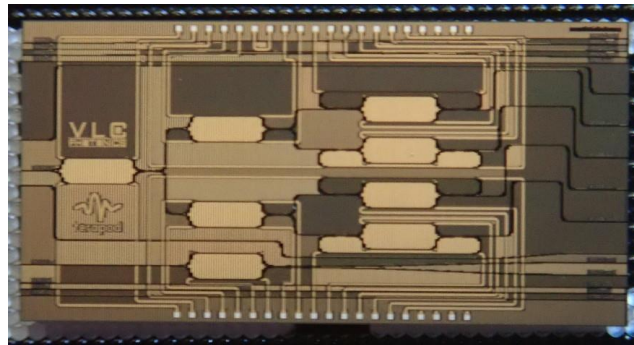


Figure 1: Picture of a TERAPOD phase distribution PIC. Die area 5x10 mm²

3.2 Characterization of test structures

Due to the low birefringence of the Silicon Nitride (SiN), horizontal and vertical polarizations propagate. In order to make relevant measurements, polarization filters were employed for the characterization of all the devices.

3.2.1 Single waveguides

A spectral dependent loss measurement was made for 4 different waveguides at both, horizontal and vertical polarizations. The recorded data is presented in Fig.9. After normalizing the measurements to the setup calibration measurement, the following data can be extracted:

- Coupling horizontal polarization (i.e. quasi-TE): 2.5 dB
- Coupling vertical polarization (i.e. quasi-TM): 7 dB

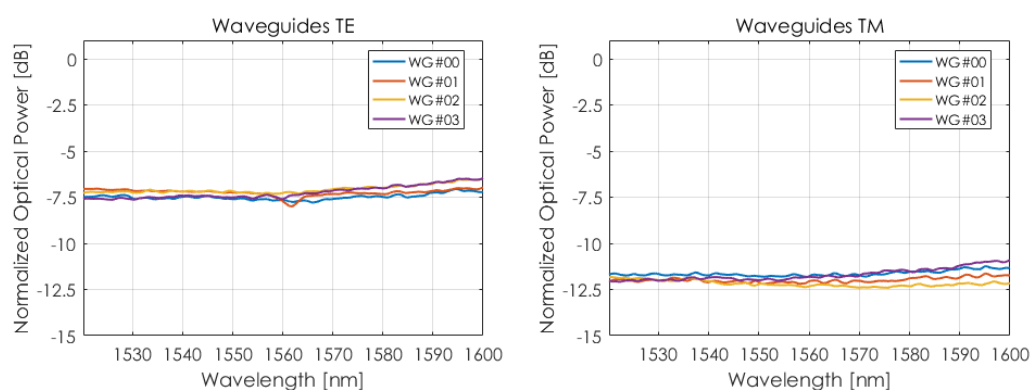


Figure 2: Straight waveguide loss per wavelength. Includes 2dB excess loss, one per filter, plus a 3dB loss from the polarization splitter. Left: quasi-TE, right: quasi-TM.



3.2.2 Multi-mode interferometer 1x2

The multi-mode interferometers, or MMIs, 1x2 are designed to provide a 50/50 splitting as presented in Figs. 3 and 4. In these figures, '00' represents input 0 to output 0, while '01' represents input 0 to output 1.

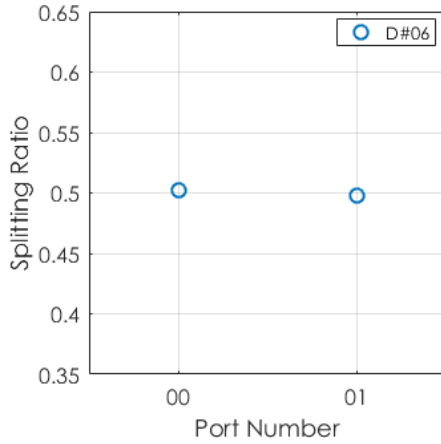


Figure 3: Splitting ratio TE input to TE output

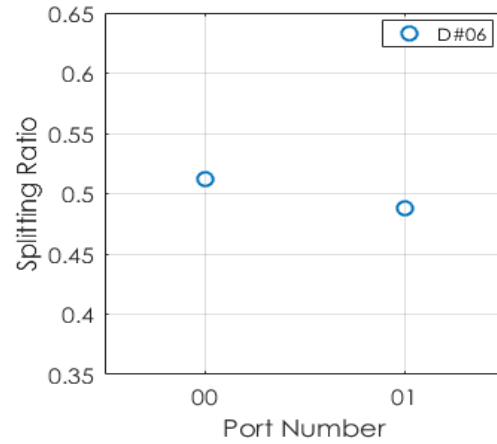


Figure 4: Splitting ratio TM input to TM output

A summary of the measurements is presented in the following table 1:

	Splitting	Deviation	Bandwidth	Total loss	Excess loss
TE-TE	50/50	<2%	~40 nm	7.8 dB	0.3 dB
TM-TM	50/50	<5%	~40 nm	12.6 dB	0.1 dB

Where total loss represents the measured loss of the device and the excess loss is the loss in a coupler besides those of the coupler. This last one consists mainly on scattering in the waveguide core walls.

3.2.3 Multi-mode interferometer 2x2

The MMIs 2x2 are designed to provide a 50/50 splitting as presented in Figs. 5 and 6. In these figures, the port numbers '00' represents input 0 to output 0, port '01' input 0 to output 1, port '10' input 1 to output 0 and port '11' input 1 to output 1.

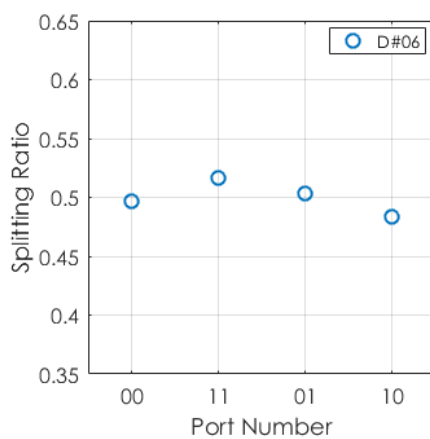


Figure 5: Splitting ratio TE input to TE output

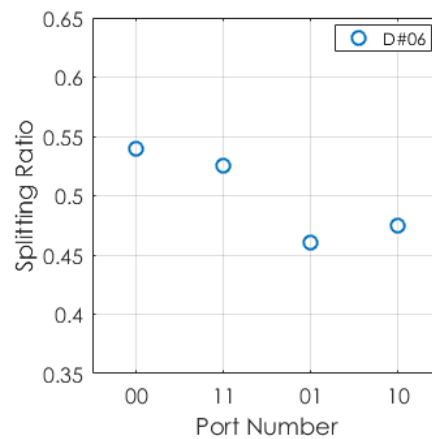


Figure 6: Splitting ratio TM input - TM output

A summary of the measurements is presented in the following table 2:

	Splitting	Deviation	Bandwidth	Total loss	Excess loss
TE-TE	50/50	<2%	~40 nm	7.6 dB	0.1 dB
TM-TM	50/50	<10%	~40 nm	12.3 dB	0.2 dB



3.2.4 MZI 1x2

A most critical component of the phase distribution PIC is the Mach-Zehnder interferometer, or MZI. In Fig. 8, at the south section (red) there is a test MZI with one input and two outputs, identical to the MZIs used in the phase distribution circuit. The coupling from single input to each output is presented in Fig.7 where the coupling from a single input is presented as a function of the current applied to a phase-controlling heater. The orange trace presents the coupling to the output 1 while the blue trace represents the coupling to the output 0.

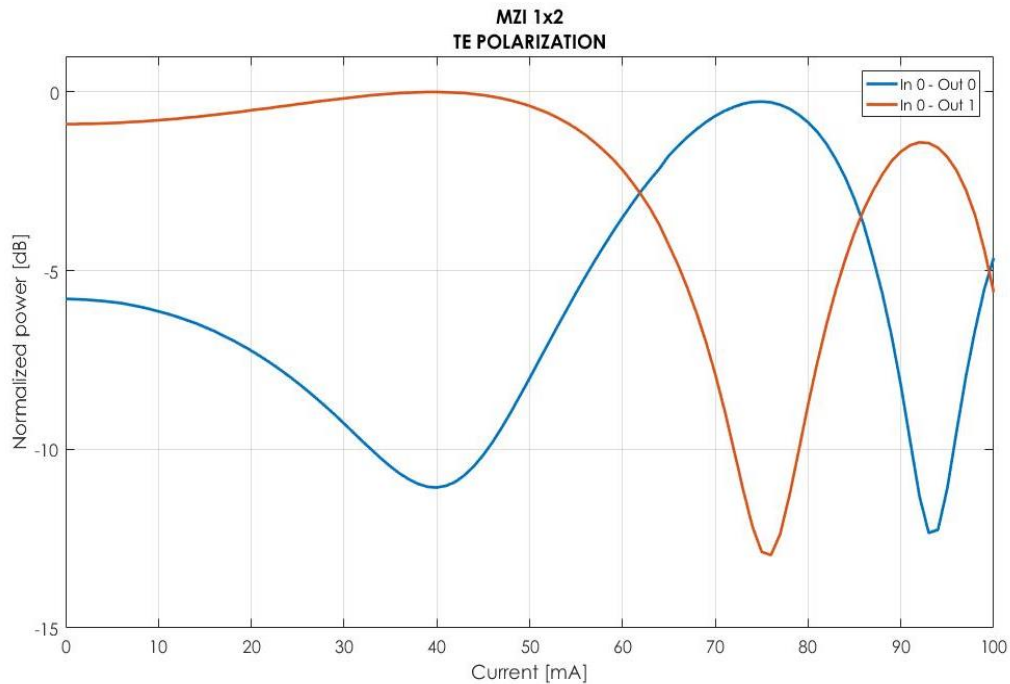


Figure 7: Mach-Zehnder in-out tuning by current steps of 1mA.

As can be seen in the figure, for a given bias current of 40mA and of 75mA, all the power is either in output 1 or 0, respectively. This provides a maximum extinction ratio of 13dB (from output to output).

3.3 Characterization of system structures

As described in deliverable 3.3, the phase distribution system is based on a tree structure represented in Fig.9. The coupling to each branch is controlled by a MZI which can be tuned by means of heating elements placed over its arms. The tuning allows to guide the light towards output 0, to output 1, or a combination of both.

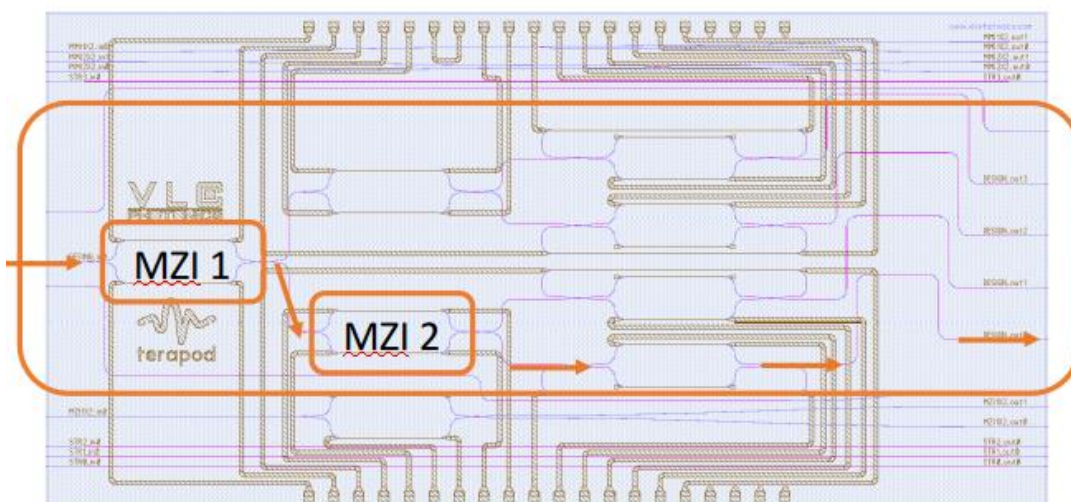


Figure 9: Cascade MZIs

By controlling only two MZIs shown in Fig.9, it is possible to guide almost all the light towards a single output. This is shown in Fig.11, where the MZIs are configured to guide light towards Output 0 (blue trace). There will be ~13dB between Output 0 to Output 1 and another 13dB between Output 2 and Output 3. As expected, the rejection between Output 0 and Output 2 is close to double the rejection of a single MZI, i.e. 24 dB. This can be seen in Fig. 10 from Output 0, the blue trace, and Output 2, the yellow trace. Output 1 and 3 receive the remaining power, in red and purple traces respectively.

The small fluctuations in the traces in Fig.11, are caused by the ring structure near each of the outputs. This is a crucial element of the system that introduces the delay.

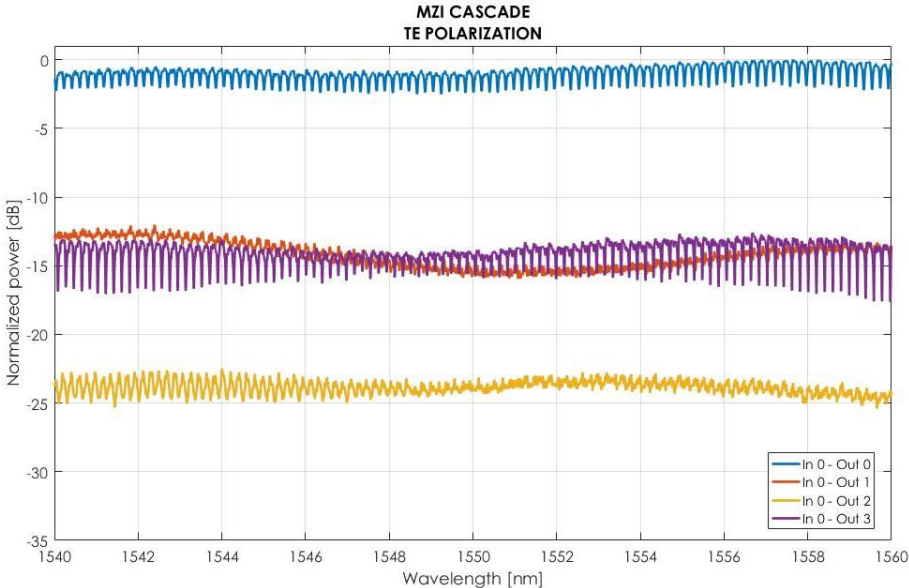


Figure 11: Measurement of power splitting for the four outputs. Controlled to send all light to Output 0.

The delay element of this system is based on a micro-ring cavity. To study the response of the rings, and thus the delay range achievable, the branches were configured such that all the light went towards Output 0 (following the orange arrows), as mentioned in the previous section. The path chosen is shown in Figure 12.

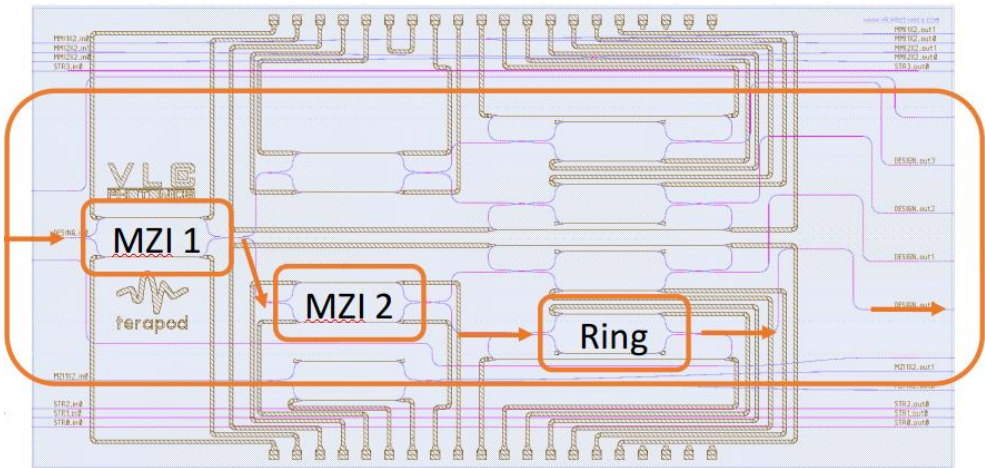


Figure 12: Light path for ring test measurements



The ring in this system is based on MMI couplers, and the coupling is controlled in the same way a

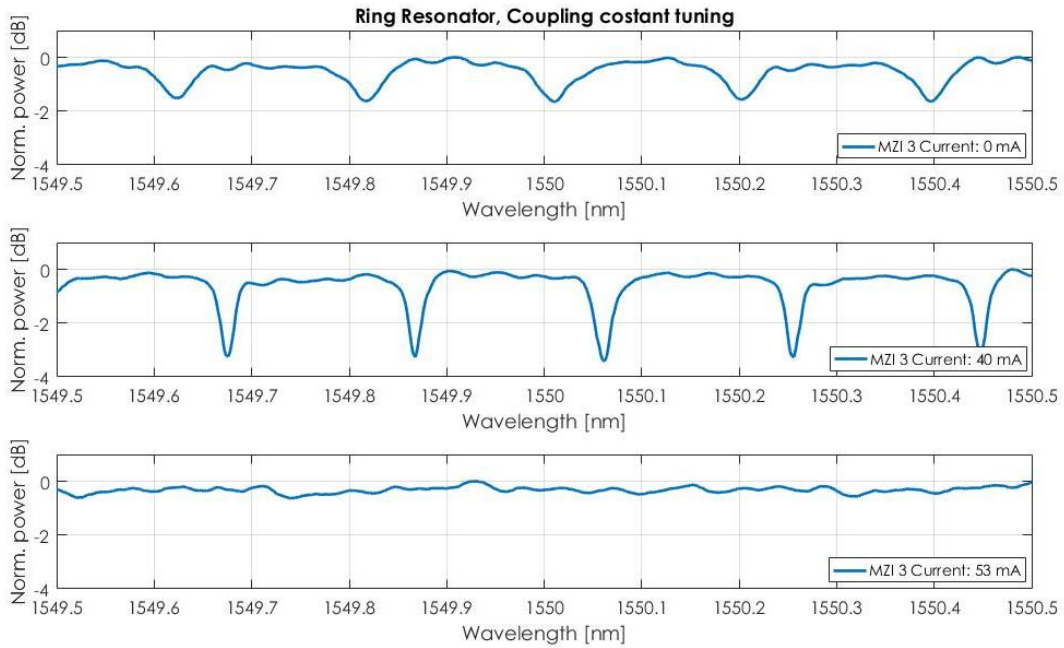


Figure 13: Ring resonator response versus wavelength

MZI is. By applying current to the heating elements, the coupling (k), can be shifted from critically coupled (k close to 0) to fully coupled (k close to 1). In Fig.13, the spectrum at the Output 0 is shown for three different coupling configurations: partially coupled ($k=0.5$) in the top, critically coupled ($k\sim 0.05$) and fully coupled ($k=1$). It is worth mentioning that the extinction ratio (depth of the peak) in the critically coupled case can be significantly higher than the one reported here since this measurement is limited by the resolution of the Optical Spectrum Analyzer (10 pm).

Given that the physical length of the ring L_{ring} is 4127 μm , the delay (L_{delay}) provided by the ring can be expressed as [1]:

$$L_{delay} = L_{ring} * F * n_{group}, \quad \text{Eq. 1}$$

where n_{group} is the group index of the light and Finesse, F , is the average number of round trips for a photon. The finesse is then defined as

$$F = \frac{FSR}{FWHM} = \frac{0.194\text{nm}}{0.022\text{nm}} = 8.81. \quad \text{Eq. 2}$$

Where FSR denotes the free spectral range while FWHM is the full width at half maximum of a resonance peak. From Eq. 1, the maximum delay achievable can be derived $L_{delay} = 76.43\text{mm}$, or a delay of 254.9 ps.

In the case of a 100GHz signal, with a free space wavelength of 2.99 mm, a possible delay of 25 times the wavelength is possible. However, this is normally not the desired situation since higher delay implies higher losses.

Alternatively and by taking advantage that the delay-bandwidth product is constant for ring resonators (equals $2/\pi$), the time delay (τ_g) can be also obtained from the FWHM, but in frequency, as [2]:

$$\tau_g = 2/(\pi FWHM(\omega)) = 231.9 \text{ ps}. \quad \text{Eq. 3}$$

This is about 23 times longer than the period of a 100 GHz signal. The difference between both results is most probably caused by the low accuracy of the FWHM measurement. However, this is still being investigated.



The length of the delay and the wavelength where the delay is applied can be easily modified by means of the heating elements. As mentioned already, one heating element can be used to control the coupling, another heating element is located over the ring and allows for control of the resonant frequency. This effect is shown in Fig. 12 where the power and spectrum are recorded while increasing the applied bias current from 0 to 60mA.

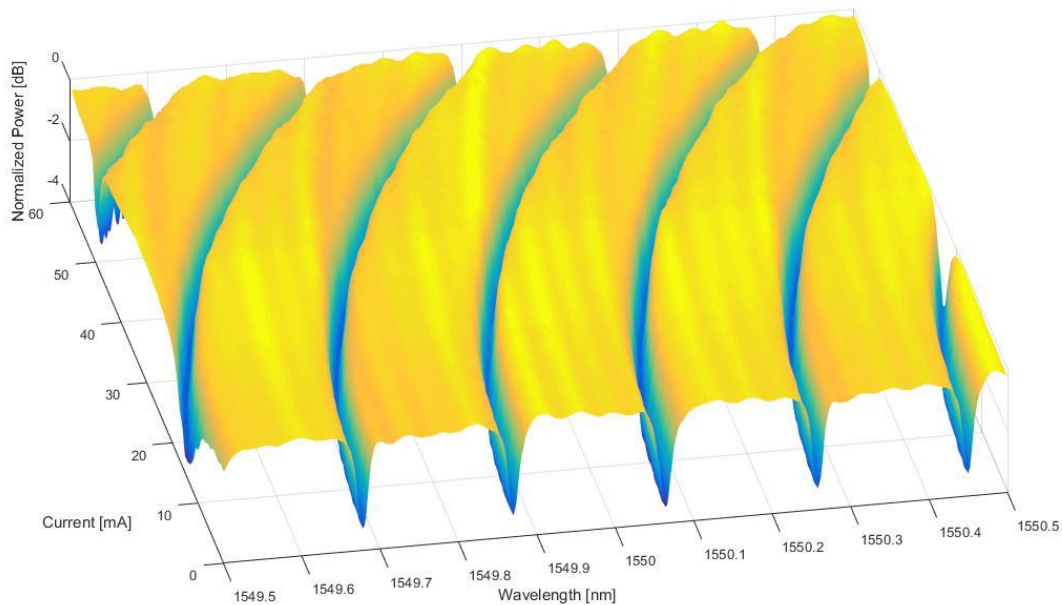


Figure 14: Ring resonator resonance tuning as a function of the applied bias current.

4 Future work

In order to improve the accuracy of the FWHM measurements a tuneable narrow linewidth laser can be utilized [3]. However, due to the large phase delay the ring resonators can provide on the GHz modulating signal, the FWHM (on an useful configuration) can be large, thus easily measurable. To further improve the control of the phase delay and provide true-time delay, two cascaded rings will be utilized as depicted in the figure below.

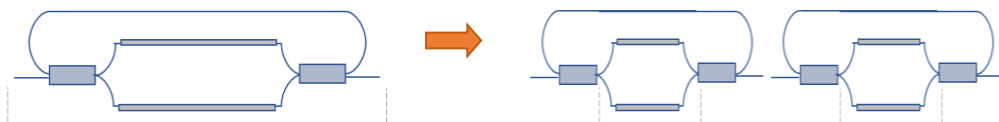


Figure 15: From one ring resonator to two shorter cascaded rings.

An alternative solution to be evaluated is to use a 3x3 MMI based ring resonator configuration, with phase shifters, as a variable external coupling. The configuration is depicted in the figure 14. This approach might allow to tune more accurately the coupling (κ) of the ring resonator, and thus the FWHM. This structure will be tested individually, to characterized how much insertion losses might add to the system.



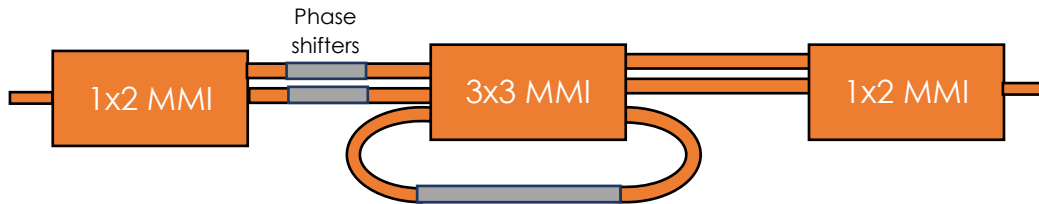


Figure 16: 3x3 MMI based ring resonator configuration.

5 Conclusion

In this document, we have presented the measurements from several different structures on the PIC. These provide sufficient information to predict the maximum delay that can be introduced to the sub-THz signal as well as a good estimate of the overall performance of the phase distribution.

It is worth mentioning that although the measurement presented in Fig. 12 is not sufficiently accurate, it can give us a good indication that the delay introduced by the ring in critical coupling is far more than the delay required for a 100GHz signal to accomplish $\pm\pi/4$ beam steering. Thus, the configuration of the ring should be done such that only a small delay (of few periods of the modulated signal) is introduced. Then by modifying the optical length of the ring, using the heating element, the required delay for beam steering can be accomplished.

[1] Douwe H. Geuzebroe et al. "*Ring-Resonator-Based Wavelength Filters.*", Springer Series in Optical Sciences book series (SSOS), volume 123, pp. 341-379. September 2006.

DOI: 10.1007/3-540-31770-8_9

[2] Roeloffzen, C. G. H. et al. "*Integrated photonic beamformer employing continuously tunable ring resonator-based delays in CMOS-compatible LPCVD waveguide technology.*", Optoelectronic Materials and Devices III vol. 7135 71351K (International Society for Optics and Photonics, 2008).

DOI: 10.1117/12.803719

[3] P. Wiersma, R. Amram. "*Characterisation of Si_3N_4 ring resonators.*", Bachelor Thesis, 2013.

Available online: https://essay.utwente.nl/63815/1/BSc_P._Wiersma_R._Amram_OPENBAAR.pdf

